Article

Cite This: *Biomacromolecules* 2019, 20, 3855−3863

pubs.acs.org/Biomac

HER2-Specific Reduction-Sensitive Immunopolymersomes with High Loading of Epirubicin for Targeted Treatment of Ovarian Tumor

Lin Ding,[†,§] Wenxing Gu,[†,‡,§] Yifan Zhang,[†] Shujing Yue,[†] Huanli Sun,[*,†] Jeroen J. L. M. Cornelissen,[‡] and Zhiyuan Zhong[*,†]

[†]Biomedical Polymers Laboratory, and Jiangsu Key Laboratory of Advanced Functional Polymer Design and Application, College of Chemistry, Chemical Engineering and Materials Science, and State Key Laboratory of Radiation Medicine and Protection, Soochow University, Suzhou 215123, P. R. China

[‡]Department of Biomolecular Nanotechnology, MESA+ Institute for Nanotechnology, University of Twente, 7500 AE Enschede, The Netherlands

Supporting Information

ABSTRACT: Monoclonal antibodies can effectively target to tumors in patients, as validated by antibody−drug conjugates (ADCs). The clinically used ADCs, nevertheless, are restricted to toxins only and suffer from low drug content, excessive use of antibody, and high cost. Here, we report on trastuzumab-decorated disulfide-cross-linked polymersomes (Tra-Ps) for specific delivery of epirubicin hydrochloride (EPI·HCl) to HER2-positive SKOV-3 ovarian tumor. EPI·HCl-loaded Tra-Ps (Tra-Ps-EPI) with a small size of 50−60 nm and varying Tra surface densities (0.5 to 2.4 Tra per Ps) were conveniently obtained via post-conjugation of thiolated trastuzumab onto the surface of maleimide-functionalized Ps-EPI with a drug loading content of 12.7 wt %. Interestingly, Tra-Ps with 1.3 trastuzumab on the surface exhibited a 6-fold higher binding affinity to the HER2 extracellular domain than that of native trastuzumab. In vitro studies revealed that Tra-Ps-EPI with long-term storage stability could rapidly release drugs under a reductive condition and efficiently deliver a large amount of EPI·HCl to HER2-positive SKOV-3 cells, leading to stronger cytotoxicity than the nontargeted Ps-EPI. Moreover, Tra-Ps-EPI displayed a long circulation time (ca. 8 h), deep tumor penetration, and superior tumor growth inhibition in SKOV-3 ovarian tumor-bearing nude mice, which were more effective than free EPI·HCl and nontargeted Ps-EPI. These HER2-specific reduction-sensitive immunopolymersomes with high loading of epirubicin emerge as an attractive treatment for HER2-positive tumors.

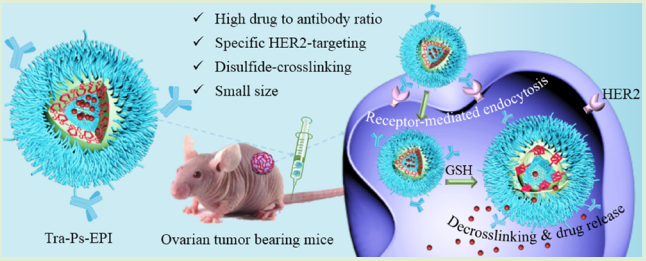

1. INTRODUCTION

Over the past decades, monoclonal antibody-based cancer therapeutics have sparked great attention as a result of their high selectivity and affinity offering precision drug delivery.[1−4] For instance, trastuzumab (Herceptin, Tra), a marketed humanized monoclonal antibody, has been clinically used as monotherapy or in combination with chemotherapeutics (such as anthracyclines, docetaxel, etc.) to treat HER2-overexpressed breast and gastric cancers.[5,6] Although an evident role in cancer therapy is observed, acquired drug resistance and severe systemic toxicity derived from chemotherapy remain to be major challenges causing high morbidity and mortality. In light of its high specificity to HER2 receptors that are overexpressed on breast, ovarian, and gastric cancer cells, Tra was further utilized as a unique targeting ligand for antibody−drug conjugates (ADCs).[7−10] FDA-approved Kadcyla (ado-trastuzumab emtansine), as a typical example, has demonstrated significant therapeutic efficacy against HER2-overexpressed metastatic breast cancers.[11] However, ADCs including Kadcyla are limited to the use of highly toxic drugs as payloads and suffer drawbacks of low drug-to-antibody ratio (3.5−4 drug molecules per antibody) and, consequently, high antibody consumption.[12,13]

To overcome the problems of ADCs, various Tra-decorated immunonanosystems have been engineered for HER2-targeted delivery of either conventional chemotherapeutics or potent warheads for ADCs.[14−17] These immunonanosystems are able to deliver high amounts of drugs using a few Tra per particle.[18−20] For example, Tra-conjugated immunoliposomes efficiently delivered paclitaxel and rapamycin to HER2-positive SK-BR-3 breast cancer cells, inducing ca. 3-fold higher toxicity in vitro and 2-fold stronger tumor inhibition rate in vivo than the nontargeted control.[21] Tra-modified docetaxel-loaded PLGA nanoparticles were constructed with a drug-to-antibody molar ratio of over 200, which was 50 times higher than that of ADCs.[22,23] Thus obtained immunoparticles realized targeted delivery of docetaxel to SK-BR-3 cancer cells, resulting in a lower half-maximal inhibitory concentration (IC_{50}) compared

Received: July 9, 2019
Revised: August 30, 2019
Published: September 12, 2019

DOI: 10.1021/acs.biomac.9b00947
Biomacromolecules 2019, 20, 3855−3863

Scheme 1. Illustration of Trastuzumab-Decorated Polymersomal Epirubicin (Tra-Ps-EPI) Based on Mal-PEG-P(TMC-DTC) and PEG-P(TMC-DTC) Copolymers for HER2-Targeted Ovarian Cancer Therapy

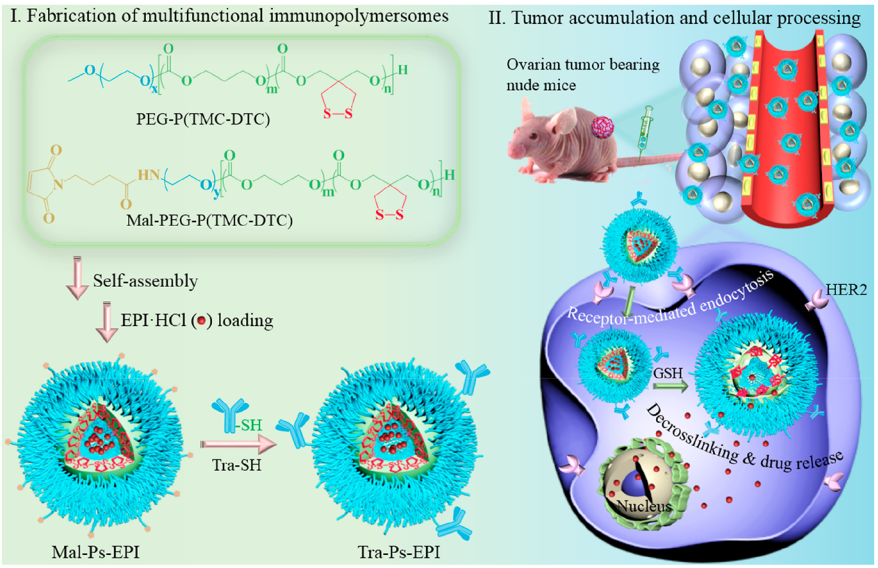

to the counterpart without Tra. HER2-targeted delivery of doxorubicin by Tra-conjugated chitosan-pluronic nanosystems was also reported with enhanced tumor accumulation and growth inhibition in SK-BR-3 breast tumor-bearing mice.[24] It should be noted, however, that the performance of Tra-decorated nanosystems is far from optimal, partly due to their poor in vivo stability, large size, and/or noncontrolled drug release.

Disulfide-cross-linking has been recently corroborated as an attractive strategy to simultaneously address the circulation stability and drug release issues of polymeric nanomedicines.[25−27] Based on dithiolane trimethylene carbonate (DTC)-containing amphiphilic copolymers, we developed robust, simple, and disulfide-cross-linked polymersomes that exhibited enhanced tumor therapy with varying drugs including doxorubicin, proteins, or siRNA.[28−30] Here, we report on small-sized, HER2-specific, and reduction-sensitive immunopolymersomes (Tra-Ps) with a high loading of epirubicin hydrochloride (EPI·HCl) for targeted treatment of SKOV-3 ovarian tumor (Scheme 1). Tra-Ps-EPI was prepared via post-conjugation of thiolated Tra on the surface of maleimide-functionalized polymersomal epirubicin. Interestingly, our results showed that Tra-Ps had a stronger binding affinity to the HER2 extracellular domain than native Tra. EPI·HCl-loaded Tra-Ps, with a high drug-to-antibody ratio of ca. 1700, revealed enhanced specificity and cellular uptake in HER2-positive SKOV-3 cells, leading to effective tumor suppression in vivo.

2. EXPERIMENTAL SECTION

2.1. Construction of EPI·HCl-Loaded Maleimide-Functionalized Disulfide-Cross-Linked Polymersomes (Mal-Ps-EPI). Mal-Ps-EPI was prepared from maleimide-functionalized poly(ethylene glycol)-*b*-poly(trimethylene carbonate-*co*-dithiolane trimethylene carbonate) (Mal-PEG-P(TMC-DTC)) and PEG-P(TMC-DTC) copolymers via a pH gradient method, as previously reported for DOX·HCl-loaded polymersomes.[28] PEG-P(TMC-DTC) (M_n = 5.0−(14.8−2.0) kg/mol, M_w/M_n = 1.1) and Mal-PEG-P(TMC-DTC) (M_n = 7.5−(15.5−2.3) kg/mol, M_w/M_n = 1.2) were synthesized according to our previous reports.[31,32] Their ^{1}H NMR spectra and GPC traces are shown in Figures S1 and S2. Typically, 50 mL of Mal-PEG-P(TMC-DTC) and PEG-P(TMC-DTC) solution in DMF (40 mg/mL, molar ratio = 5/95) was injected into 450 mL of stirred citrate buffer (pH 4.0, 10 mM). Concentrated sodium phosphate was added to adjust the pH to 7.8 followed by addition of 80 mL of EPI·HCl (5 mg/mL) and overnight incubation (37 °C, 200 rpm). Mal-Ps-EPI was purified and concentrated to a Ps concentration of 20 mg/mL using a Pellicon tangential flow filtration system (MWCO = 5000 Da, Millipore). Size distribution of Mal-Ps-EPI was investigated using dynamic light scattering (DLS). Drug loading efficiency (DLE) and drug loading content (DLC) were calculated based on the EPI·HCl amount determined via UV−vis using the formulas as follows

$$\mathrm{DLE}(\%) = \frac{\text{weight of loaded drug}}{\text{weight of drug in feed}} \times 100$$

$$\mathrm{DLC}(\text{wt }\%) = \frac{\text{weight of loaded drug}}{\text{total weight of loaded drug and polymer}} \times 100$$

Ps-EPI was fabricated using PEG-P(TMC-DTC) only under otherwise the same procedure as Mal-Ps-EPI. Blank polymersomes (Ps and Mal-Ps) were constructed similarly by directly injecting polymer solution to phosphate buffer (PB, pH 7.4, 10 mM) followed by dialysis (MWCO = 3500 Da) against PB.

2.2. Fabrication of Trastuzumab-Decorated Polymersomal EPI (Tra-Ps-EPI). Tra-Ps-EPI was fabricated via Michael addition of thiolated trastuzumab (Tra-SH) with Mal-Ps-EPI. To obtain Tra-SH, Tra (1.0 mg, 25 mg/mL) was incubated with 10-fold or 20-fold molar excess of 2-iminothiolane (2 mg/mL, PB with 5 mM EDTA, pH 8.0) under constant shaking for 1 h at 25 °C. The resulting Tra-SH was purified by a Zeba spin desalting column, and its concentration was calibrated using the Tra standard curve measured by HPLC (150 mM PB/ACN = 90:10; flow rate, 1 mL/min; 214 nm). The thiolation degree of Tra-SH was quantified using Ellman's assay. Briefly, 900 μL of Tra-SH solution (1 mg/mL) was incubated with 100 μL of DTNB (3.96 mg/mL) for 15 min at room temperature followed by absorption measurement at 412 nm with UV−vis. The thiol functionality of Tra-SH was calculated to be ca. 2.7 thiol groups per Tra based on the glutathione (GSH) standard curve with concentrations ranging from 0.01 to 0.1 mM.

Freshly obtained Tra-SH with 10-fold molar excess of 2-iminothiolane was immediately added to the Mal-Ps-EPI dispersion (20 mg/mL) with molar ratios of Tra-SH to Mal preset as 1:6, 1:3, and 1:1. After overnight reaction at 37 °C, Tra-Ps-EPI was washed

DOI: 10.1021/acs.biomac.9b00947
Biomacromolecules 2019, 20, 3855−3863

three times with PB (pH 7.4, 10 mM) by ultracentrifugation (70 krpm, 40 min) to remove free Tra-SH. The collected supernatants were analyzed by HPLC to determine the amount of unconjugated Tra-SH based on which we determined the conjugation efficiency. To further determine the Tra density on the surface of polymersomes, the molecular weight and aggregation number of Mal-Ps were measured via static light scattering (SLS). The number of Tra per polymersome was calculated according to the following formula

$$\text{number of Tra per Ps} = \frac{\text{weight of conjugated Tra/molecular weight of Tra}}{\text{weight of polymersomes/molecular weight of each polymersome}}$$

The size and PDI of Tra-Ps-EPI were measured and further tracked over 15 days of storage in the fridge by DLS. Tra-functionalized blank polymersomes (Tra-Ps) were prepared similarly to Tra-Ps-EPI. The secondary structure of Tra decorated on the polymersomes was detected using the circular dichroism spectrum (CD).

2.3. Binding Affinity of Tra-Ps to the HER2 Extracellular Domain. The binding affinity and kinetics of Tra-Ps or free Tra with the HER2 extracellular domain ($HER2_{ECD}$) were followed by surface plasma resonance (SPR, Biacore T200) at 25 °C. $HER2_{ECD}$ protein was coupled to a CM5 chip by an amine coupling kit using sodium acetate (pH 4.5, 10 mM) as the immobilization buffer. In brief, carboxylic groups of CM5 chip were activated with a solution of EDC (75 mg/mL) and NHS (12 mg/mL) at a flow rate of 10 μL/min for 10 min. Then, $HER2_{ECD}$ protein solution (4 μg/mL) was injected and immobilized on the chip to achieve a final resonance units (RU) value of 165.6. Ethanolamine·HCl was used to block the other channel and served as a reference. HBS-EP+ (pH 7.4, 10 mM HEPES with 150 mM NaCl, 3 mM EDTA, and 0.05% P-20) was used as the running buffer. All buffers were filtered through a 0.22 μm filter prior to use. For binding assay, Tra-Ps or free Tra with Tra concentrations ranging from 3.1 to 50.0 μg/mL were analyzed. Ps with a concentration of 4 mg/mL was utilized as a control. Samples for kinetic/affinity studies were run at a flow rate of 5 μL/min followed by a 2 min waiting period for dissociation before chip regeneration. Data were processed using Biacore T200 Evaluation Software version 2.0.

2.4. Assessment of HER2 Expression Levels of Tumor Cells. SKOV-3, MDA-MB-231, and BT474 human cancer cells were planted into a six-well plate with a density of 1×10^6 cells per well and cultured for 24 h. Cells were then trypsinized, centrifuged, and resuspended in 100 μL of phosphate-buffered saline (PBS) to obtain single-cell suspensions, followed by addition of 10 μL of anti-HER2 antibody-FITC to incubate for 30 min at 4 °C. Afterward, cells were centrifuged (1000 rpm, 3 min), washed three times with PBS, and finally dispersed in 500 μL of PBS for flow cytometry analysis using a BD FACS Calibur flow cytometer (Becton Dickinson, USA). At least 1×10^4 cells were analyzed for each sample, and data were processed using FlowJo_10 software.

2.5. Cellular Uptake of EPI·HCl-Loaded Polymersomes. The cellular uptake of Tra-Ps-EPI and Ps-EPI was studied by confocal laser scanning microscopy (CLSM) using both HER2-positive SKOV-3 cells and HER2-negative MDA-MB-231 cells. Cells were planted onto glass slides containing 24-well plate (8×10^4 cells/well) and allowed to adhere for 1 day. Tra-Ps-EPI and Ps-EPI were then added separately to maintain a final EPI·HCl concentration of 11.2 μg/mL. After 4 h incubation at 37 °C, adhered cells were gently washed three times with PBS, fixed using 4% paraformaldehyde for 20 min, and washed three times with PBS. Cell nuclei were stained with 4,6-diamidino-2-phenylindole (DAPI, 5 μg/mL) for 3 min followed by six times washing with PBS. Glass slides with stained cells were collected and mounted onto microscope slides for CLSM measurements.

2.6. MTT Assays. The cytotoxicity of Tra-Ps-EPI and Ps-EPI against HER2-positive SKOV-3 cells and HER2-negative MDA-MB-231 cells was evaluated by MTT assays. Cells were planted onto 96-well plates (3000 cells/well) for 1 day. Twenty microliters of Ps-EPI or Tra-Ps-EPI in PBS was added with final EPI·HCl concentrations of 0.001, 0.01, 0.05, 0.1, 0.5, 1, 5, 10, and 20 μg/mL. After 4 h incubation, the medium was replaced by 100 μL of fresh medium followed by another 68 h incubation. Ten microliters of 3-(4,5-dimethylthiazol-2-yl)-2,5-diphenyltetrazolium bromide (MTT) solution (5 mg/mL in PBS) was added into each well and incubated for 4 h. The generated formazan in each well was dissolved in DMSO (150 μL) upon careful removal of the medium, and the absorbance at 570 nm was measured using a microplate reader (Thermo, ELx808IU). Cell viability (%) was relative to the control cells incubated with PBS only and calculated by comparing their absorbance at 570 nm.

2.7. In Vivo Pharmacokinetics, ex Vivo Imaging, and Tumor Penetration. All animal experiments were performed according to the protocols approved by Laboratory Animal Center and Animal Care and Use Committee of Soochow University. For the pharmacokinetics studies, Tra-Ps-EPI or Ps-EPI with an EPI·HCl dosage of 11.2 mg/kg was intravenously injected to female BALB/c mice weighing around 20 g ($n = 3$). At predetermined time points (0.08, 0.16, 0.25, 0.5, 1, 2, 4, 6, 8, 12, and 24 h), blood samples were collected into heparinized tubes and subjected to centrifugation (3000 rpm, 10 min) to take out 10−15 μL of plasma to incubate overnight with 0.75 mL of DTT solution in DMF (20 mM) for extracting EPI·HCl. EPI·HCl concentration in the supernatant was measured via a fluorescence spectrophotometer (excitation, 488 nm; emission, 560 nm). The blood circulation half-lives ($t_{1/2,\beta}$) were obtained according to the following second-order exponential decay fits: $y = A_1 \times \exp(-x/t_1) + A_2 \times \exp(-x/t_2)$ and $t_{1/2,\beta} = 0.693 \times t_2$.

The tumor targetability and penetration behavior of Tra-Ps-EPI were evaluated via ex vivo imaging and immunofluorescence analysis, respectively. SKOV-3 tumor-bearing mice with tumor volumes of ca. 200−300 mm^3 were administrated with 200 μL of Tra-Ps-EPI or Ps-EPI via tail vein injection. For ex vivo imaging, tumors and major organs were harvested at 8 h to acquire EPI·HCl fluorescence images using a near-infrared fluorescence imaging system (IVIS Lumina II) at an excitation of 488 nm and an emission of 560 nm. For the tumor penetration study, tumors were harvested at 24 h after injection, fixed with 4% paraformaldehyde, embedded in paraffin, and sliced. Blood vessels were then incubated with rat monoclonal anti-mouse CD31 antibody and stained by Alexa Fluor 647-conjugated goat anti-rat secondary antibody. Cell nuclei were stained by DAPI for CLSM measurements.

2.8. In Vivo Antitumor Efficacy. The in vivo therapeutic efficacy of Tra-Ps-EPI, Ps-EPI, and free EPI·HCl was investigated in SKOV-3 ovarian tumor-bearing mice. The different formulations were administrated at an EPI·HCl dosage of 11.2 mg/kg via a tail vein on day 0, when the average tumor volume of each group ($n = 5$) reached about 150 mm^3. The drug administration was repeated every 4 days for six injections in total except for free EPI·HCl. PBS was injected as a control. Tumor growth and the weight of mice were monitored every 2 days, wherein tumor volumes (V) were calculated from the tumor length (L) and width (W) measured using calipers ($V = 0.5 \times L \times W^2$). On day 30, tumors from all the mice were collected and weighed. Meanwhile, tumor and major organs from one mouse of each group were harvested and stained with hematoxylin and eosin (H&E) for histological analysis.

2.9. Statistical Analysis. All data were presented as mean ± standard deviation (SD). Ordinary one-way ANOVA was utilized to compare three or more groups, when the result was significant ($p < 0.05$), and Tukey's post hoc test was then performed for all pairwise comparisons. $^*p < 0.05$, $^{**}p < 0.01$, and $^{***}p < 0.001$.

3. RESULTS AND DISCUSSION

3.1. Fabrication of Trastuzumab-Decorated Polymersomes. Trastuzumab-modified polymersomes (Tra-Ps) were obtained via coassembly of 95 mol % PEG-P(TMC-DTC) with 5 mol % Mal-PEG-P(TMC-DTC) followed by Michael addition with thiolated trastuzumab (Tra-SH). Maleimide-functionalized polymersomes (Mal-Ps) showed an average size of 49.2 nm and an aggregation number of ca. 447, as determined by DLS and SLS, respectively (Figure S3). By setting the molar ratios of Traut's reagent to antibody at 10:1

DOI: 10.1021/acs.biomac.9b00947
Biomacromolecules 2019, 20, 3855−3863

and 20:1, Tra-SH conjugates with an average of 2.7 and 5.4 thiol groups per Tra were prepared, respectively, as determined by Ellman's assay. The former one was utilized for the following studies to maintain a relatively high activity and targetability of Tra. Overnight treatment of Mal-Ps with Tra-SH at Tra-to-Mal molar ratios of 1:30, 1:12, and 1:6 yielded Tra$_x$-Ps with Tra densities of 0.5, 1.3, and 2.5 per polymersome (x means Tra density), respectively, as quantified by HPLC (Table S1). Notably, all Tra-Ps exhibited similar sizes (50.4−51.2 nm) and zeta potentials (−0.38 to 0.09 mV) to that of Mal-Ps (49.2 nm, −2.27 mV) and Ps (48.9 nm, −1.23 mV). Circular dichroism (CD) spectra revealed that Tra decorated on the surface of polymersomes possessed a similar secondary structure as native Tra (Figure 1A).

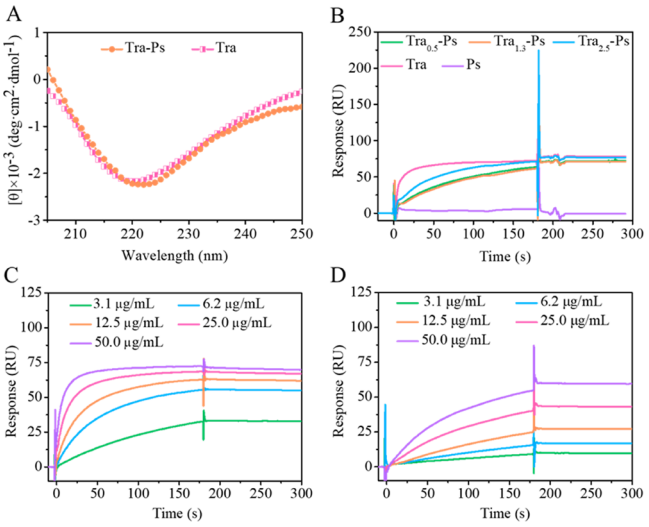

Figure 1. (A) Secondary structure of native Tra and Tra-Ps determined by CD. (B) SPR sensograms representing the interactions of Tra$_x$-Ps with different Tra densities and native Tra to HER2$_{ECD}$ at a Tra concentration of 25.0 μg/mL. (C) Binding kinetics of free Tra to HER2$_{ECD}$. (D) Binding kinetics of Tra$_{1.3}$-Ps to HER2$_{ECD}$.

To test the affinity of Tra-Ps binding to HER2, the HER2 extracellular domain (HER2$_{ECD}$) was modified on the surface of a CM5 chip via EDC/NHS chemistry to achieve a final response of 165.6 RU, as determined by SPR. Binding assays revealed that Tra$_x$-Ps, regardless of Tra density, showed similar binding responses to free Tra with RU values of about 74 when fixing the Tra concentration at 25.0 μg/mL (Figure 1B). The relatively slow binding rate of Tra-Ps is most possibly due to their slower diffusion compared to free Tra. On the contrary, no appreciable binding of unmodified Ps on the chip was observed even at a concentration of 4 mg/mL, which was over 4-fold higher than that of Tra-Ps. These results indicated that Tra was successfully conjugated to the surface of Mal-Ps and its binding affinity to HER2$_{ECD}$ was significantly improved. To further quantify the binding of Tra-Ps and free Tra to HER2$_{ECD}$, a series of Tra$_{1.3}$-Ps and Tra with Tra concentrations of 3.1 to 50.0 μg/mL were flowed over the chip, and the kinetic constants were measured (Figure 1C,D). It was found that Tra-Ps displayed about a 5-fold lower association constant (K_a) and a 29-fold lower dissociation constant (K_d) than those of native Tra, yielding a much smaller equilibrium dissociation constant (K_D, 7 pM versus 42 pM) and thus stronger binding affinity (Table 1). This is in line with the reports stating that K_D for monoclonal antibodies with antigens is in the order of picomolar[33,34] and antibody-decorated nanoparticles bear higher binding affinity than free antibodies possibly as a result of multivalent effects.[35,36]

Table 1. Affinity Constants of Native Tra and Tra-Ps Binding to HER2$_{ECD}$

sample	K_a (1/Ms)	K_d (1/s)	K_D (M)
Tra	6.7×10^4	2.8×10^{-6}	4.2×10^{-11}
Tra$_{1.3}$-Ps	1.4×10^4	9.6×10^{-8}	6.9×10^{-12}

3.2. Preparation of Trastuzumab-Decorated EPI·HCl-Loaded Polymersomes. Utilizing the pH gradient method that was previously applied for DOX·HCl-loaded polymersomes and liposomes,[37,38] a large batch of Ps-EPI (50.8 nm) and Mal-Ps-EPI (54.2 nm) with a DLC of 12.7 wt % was acquired at a theoretical DLC of 16.7 wt %. The loading capability of polymersomes for EPI·HCl was similar to that for DOX·HCl as a result of their similar physicochemical properties.[39,40]

Mal-Ps-EPI was then reacted with Tra-SH overnight as that for blank polymersomes with subsequent ultracentrifugation, yielding Tra-Ps-EPI with negligible EPI·HCl leakage during the fabrication (Figure 2A). HPLC analysis of the collected supernatant indicated that surface densities of thus obtained Tra-Ps-EPI were 0.5, 1.4, and 2.4 at Tra-to-Mal feeding molar ratios of 1:6, 1:3, and 1:1, respectively. Figure 2B and Table 2 reveal that all Tra-Ps-EPI had a similar size (53.2−58.3 nm), size distribution, and zeta potential, which were close to those of Ps-EPI and Mal-Ps-EPI. Moreover, Tra-Ps-EPI exhibited high stability during storage in the fridge over a period of 15 days (Figure 2C). In vitro release studies confirmed that Tra-Ps-EPI released 93% of EPI·HCl in 24 h under a reductive condition (10 mM GSH), while ca. 35% release was observed in PB (pH 7.4, 10 mM) only (Figure 2D). This release profile is similar to that of Ps-EPI and also other disulfide-cross-linked polymeric nanomedicines.[41,42]

3.3. Cellular Uptake and in Vitro Antitumor Activity of Tra-Ps-EPI. HER2 expression levels of several human cancer cells including BT474 breast cancer cells, SKOV-3 ovarian cancer cells, and MDA-MB-231 triple-negative breast cancer cells were detected by flow cytometry using anti-HER2 antibody-FITC. It was found that HER2 is highly expressed on the surface of SKOV-3 and BT474 cells, while MDA-MB-231 cells showed low HER2 expression (Figure 3), which is in line with previous reports.[43−46] We hereafter utilized MDA-MB-231 cells as a HER2-negative control.

Cellular uptake and intracellular drug release behavior of Tra$_{1.4}$-Ps-EPI in HER2-positive SKOV-3 and HER2-negative MDA-MB-231 cells were followed by CLSM. The acquired images showed strong EPI·HCl fluorescence inside SKOV-3 cells particularly in the nuclei after 4 h incubation with Tra-Ps-EPI, supporting its efficient cellular uptake as well as rapid EPI·HCl release and nuclei accumulation (Figure 4A). By contrast, Ps-EPI-treated SKOV-3 cells displayed weak EPI fluorescence. These results corroborated the enhanced cellular uptake and active targeting ability of Tra-Ps-EPI, as also observed for other Tra-functionalized nanosystems.[47−51] For HER2-negative MDA-MB-231 cells, the EPI fluorescence intensity was almost the same for Tra-Ps-EPI and Ps-EPI (Figure 4B), similar to Ps-EPI-treated SKOV-3 cells (Figure 4A), confirming the high HER2 specificity of Tra-Ps-EPI. We further analyzed the mean EPI fluorescence intensity in the cells. The results showed that SKOV-3 cells incubated with Tra-Ps-EPI had ca. 6-fold higher

DOI: 10.1021/acs.biomac.9b00947
Biomacromolecules 2019, 20, 3855−3863

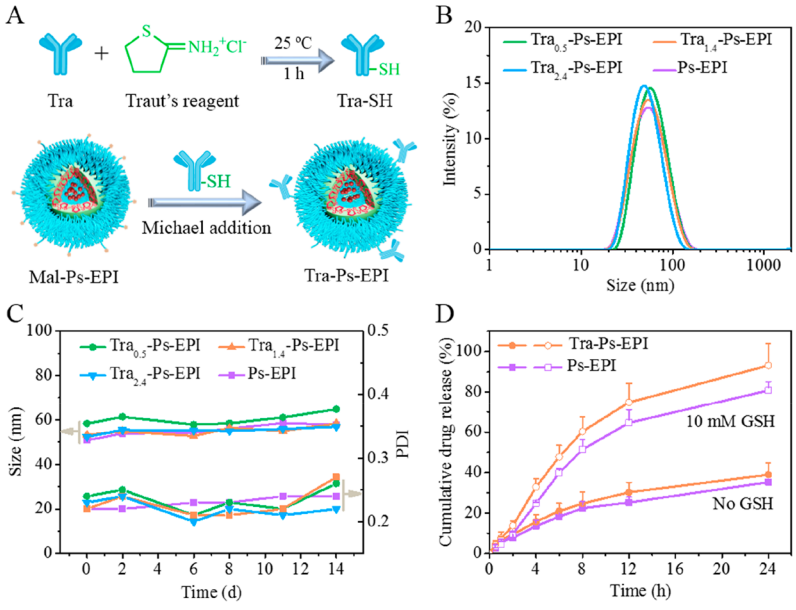

Figure 2. (A) Preparation and (B–D) characteristics of Tra-Ps-EPI. (B) Size distribution determined using DLS. (C) Storage stability at 4 °C for 15 days. (D) In vitro EPI·HCl release from Tra-Ps-EPI and Ps-EPI either in the presence or in the absence of 10 mM GSH (n = 3).

Table 2. Characterization of EPI·HCl-Loaded Polymersomes with Varying Tra Surface Densities in PB (pH 7.4, 10 mM)

		conjugated Tra				
polymersome	molar ratio of Tra to Mal	μg/mg Ps[a]	number per Ps	size (nm)[b]	PDI[b]	ζ (mV)[c]
Ps-EPI				50.8	0.22	−4.58
$Tra_{0.5}$-Ps-EPI	1:6	7.2	0.5	58.3	0.24	−5.32
$Tra_{1.4}$-Ps-EPI	1:3	21.4	1.4	55.4	0.22	−2.92
$Tra_{2.4}$-Ps-EPI	1:1	35.2	2.4	53.2	0.23	−2.60

[a]Measured by HPLC. [b]Determined by DLS. [c]Determined by a Zetasizer Nano-ZS equipped with an electrophoresis cell.

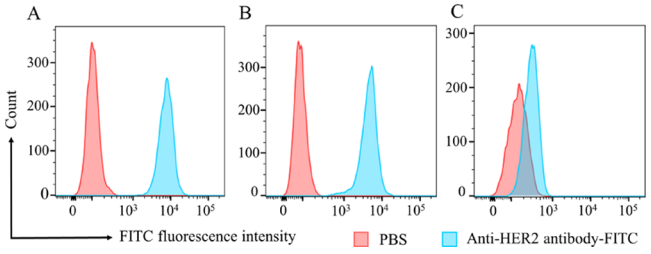

Figure 3. Flow cytometry analysis of HER2 expression levels on the membrane of (A) BT474, (B) SKOV-3, and (C) MDA-MB-231 cells using anti-HER2 antibody-FITC.

EPI fluorescence than those with Ps-EPI and MDA-MB-231 cells treated with Tra-Ps-EPI or Ps-EPI (Figure 4C).

MTT assays revealed that Tra-Ps-EPI, regardless of the Tra density, induced ca. 2-fold higher toxicity toward HER2-positive SKOV-3 cells than the nontargeted Ps-EPI control (Figure 5A), corroborating the enhanced intracellular delivery and release of EPI·HCl. This is consistent with the SPR data that showed comparable binding affinity of Tra-Ps-EPI with different Tra densities. In contrast, similar anticancer activity to HER2-negative MDA-MB-231 cells was observed for Ps-EPI and $Tra_{1.4}$-Ps-EPI (Figure 5B), which displayed an about 5-fold higher IC_{50} (11.0 μg/mL) than Tra-Ps-EPI against SKOV-3 cells. These results further support the fact that Tra improves the specific cellular uptake and cytotoxicity of Ps-EPI in HER2-positive cells. Importantly, blank Tra-Ps and native Tra were nontoxic against SKOV-3 cells even at a Ps concentration of 0.5 mg/mL and corresponding Tra concentration of 10 μg/mL, which was much lower than the effective concentration in SKOV-3 cells (Figure 5C,D).[52,53] This indicated that the higher toxicity of Tra-Ps-EPI than Ps-EPI was mainly due to the Tra-directed targeting effect.

3.4. In Vivo Pharmacokinetics, ex Vivo Imaging, and Tumor Penetration. The stability in vivo is a critical issue for achieving long circulation and therefore tumor accumulation of nanomedicines. Hence, the pharmacokinetics of Ps-EPI and Tra-Ps-EPI were first investigated using BALB/c mice. As shown in Figure 6A, Tra-Ps-EPI exhibited a long elimination half-life of 8.0 h, which is comparable with the nontargeted Ps-EPI and other PEG-P(TMC-DTC)-based disulfide-cross-linked polymersomal drugs,[54,55] while it is markedly longer than that of free EPI·HCl.[56,57] Biodistribution of Tra-Ps-EPI and Ps-EPI in subcutaneous SKOV-3 ovarian tumor-bearing nude mice was evaluated at 8 h post-injection. The ex vivo fluorescence images displayed that Tra-Ps-EPI accumulated more in the tumor with stronger EPI·HCl fluorescence than that of nontargeted Ps-EPI control (Figure 6B).

Tumor penetration is also a critical step for nanomedicines to realize efficient cancer treatment.[58−61] Monoclonal antibodies were reported with limited tumor penetration as a result of a specific binding site barrier and/or possible nonspecific interactions with extracellular components.[62] To evaluate the effect of Tra decoration on the tumor penetration performance of Ps-EPI, the distribution of Tra-Ps-EPI and Ps-EPI in the

DOI: 10.1021/acs.biomac.9b00947
Biomacromolecules 2019, 20, 3855−3863

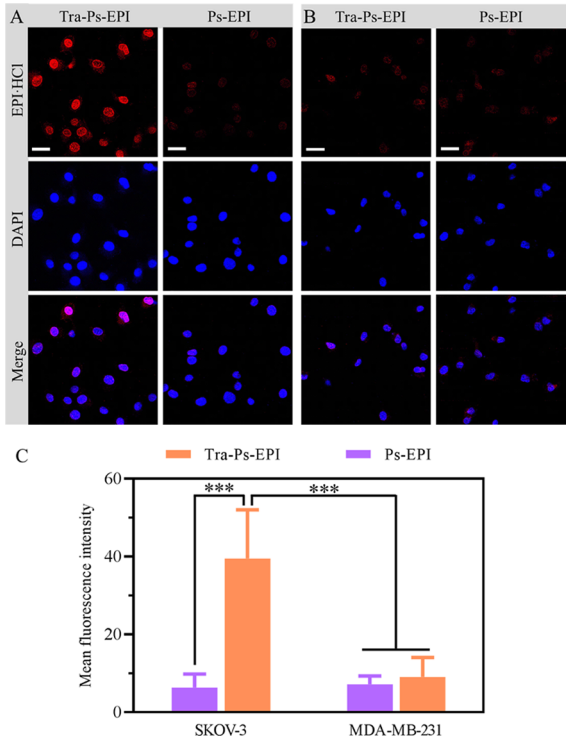

Figure 4. CLSM images of (A) HER2-positive SKOV-3 and (B) HER2-negative MDA-MB-231 cells following 4 h incubation with Tra-Ps-EPI or Ps-EPI (scale bars: 25 μm). (C) Mean fluorescence intensity of EPI·HCl in the cell nuclei analyzed by ImageJ. ***p < 0.001.

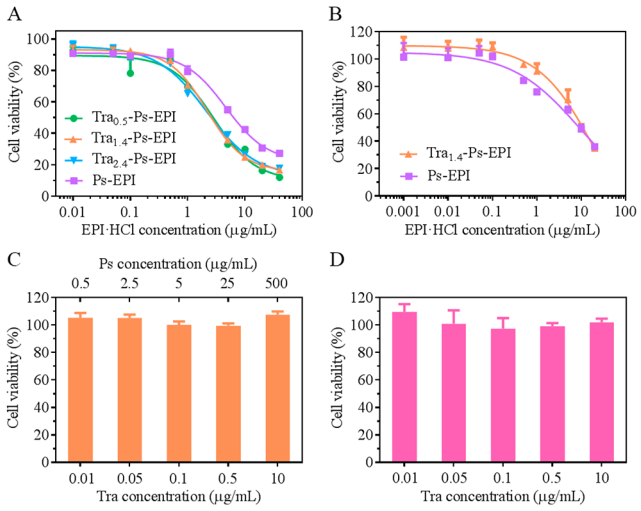

Figure 5. Cell viability of (A) HER2-positive SKOV-3 and (B) HER2-negative MDA-MB-231 cells after treatment with Tra-Ps-EPI and Ps-EPI, respectively (n = 4). MTT assays of (C) blank Tra-Ps and (D) free Tra in SKOV-3 cells (n = 4). Cells were incubated with different formulations for 4 h followed by another 68 h incubation in fresh medium.

SKOV-3 tumor was examined at 24 h post-intravenous injection using CLSM with immunofluorescent staining. As shown in Figure 6C and Figure S4, Tra-Ps-EPI was distributed throughout the whole tumor slice and even with stronger EPI·HCl fluorescence perfused in the tumor interstitium up to 125 μm away from tumor vessels compared to Ps-EPI. This indicated that Tra-Ps-EPI has better tumor-penetrating ability,

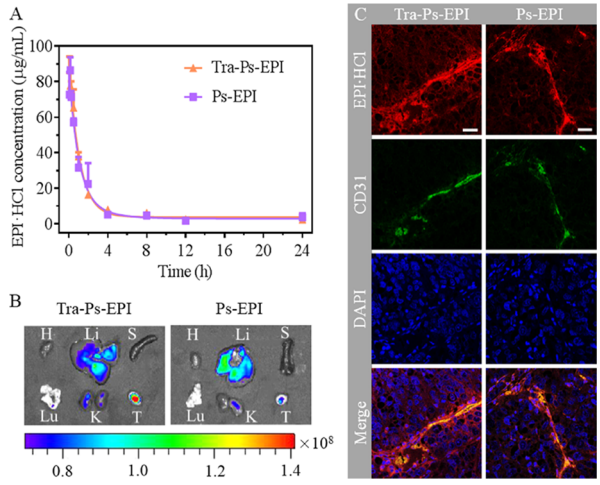

Figure 6. In vivo pharmacokinetics, biodistribution, and tumor penetration studies of Tra-Ps-EPI and Ps-EPI (dosage: 11.2 mg EPI·HCl equiv/kg). (A) Pharmacokinetics in BALB/c mice after intravenous injection (n = 3). (B) Ex vivo EPI·HCl fluorescence images of tumors and major organs harvested from SKOV-3 tumor-bearing nude mice at 8 h post-intravenous injection (H, heart; Li, liver; S, spleen; Lu, lung; K, kidney; T, tumor). (C) Penetration behavior in SKOV-3 tumor tissue studied by CLSM (CD31: pseudocolored in green). Scale bars are 25 μm.

likely due to its enhanced binding affinity toward tumor cells. The longer circulation, higher tumor accumulation, and efficient tumor penetration laid the foundation of Tra-Ps-EPI for HER2-targeted tumor therapy.

3.5. Antitumor Efficacy of Tra-Ps-EPI in SKOV-3 Ovarian Tumor-Bearing Mice. The in vivo therapeutic efficacy of Tra-Ps-EPI was investigated using subcutaneous SKOV-3 ovarian tumor-bearing nude mice with an EPI·HCl dosage of 11.2 mg/kg. Tra-Ps-EPI with repeated injections every 4 days for six times in total largely suppressed the tumor growth over a period of 30 days (***p < 0.001 versus PBS) (Figure 7A,B). Its tumor growth inhibition effect was much stronger than that induced by nontargeted Ps-EPI (**p < 0.01), supporting the fact that Tra decoration significantly improved the tumor-targeting ability of Ps-EPI and enhanced the therapeutic efficacy. Free EPI·HCl, although exhibited some tumor inhibition effect (*p < 0.05 versus PBS), caused significant body weight loss (>15%) during the treatment even with only three injections, revealing its high systemic toxicity against nude mice (Figure 7A–C). Importantly, no obvious body weight change was detected for polymersomal EPI (Tra-Ps-EPI and Ps-EPI)-treated groups, indicating their high tolerability in nude mice. The images of tumor harvested on day 30 (Figure 7D) confirmed the same trend of tumor volume as that in Figure 7B (PBS > Ps-EPI > EPI·HCl > Tra-Ps-EPI), further corroborating the superior antitumor effect of targeted Tra-Ps-EPI. Compared with other chemotherapeutics-based polymeric nanomedicines targeting to EGFR, CD44, or $\alpha_v\beta_3$ integrins, Tra-Ps-EPI induced the obviously higher tumor inhibition rate of SKOV-3 ovarian tumor-bearing mice.[63−66] Moreover, apparent tumor cell shrinkage and incomplete cell membranes were observed in the H&E-stained tumor tissue for Tra-Ps-EPI, which was significantly more than that of Ps-EPI- and free EPI·HCl-treated group (Figure 7E). It should further be noted that polymersomal EPI caused little damage to the

DOI: 10.1021/acs.biomac.9b00947
Biomacromolecules 2019, 20, 3855−3863

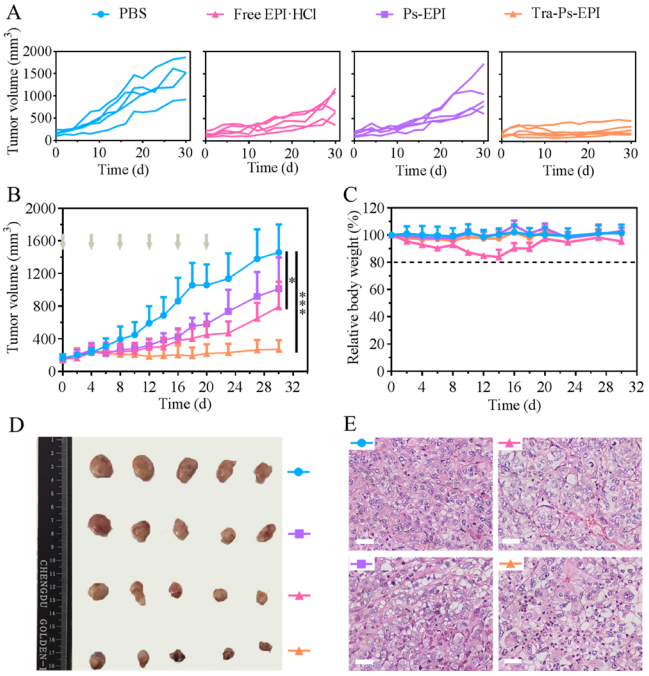

Figure 7. In vivo antitumor effect of Tra-Ps-EPI in SKOV-3 tumor-bearing nude mice. Ps-EPI, free EPI·HCl, and PBS groups were used as controls. (A) Individual and (B) average tumor volume changes (n = 5). *p < 0.05, and ***p < 0.001. (C) Body weight changes of mice within 30 days. (D) Photos of isolated tumor lumps on day 30. (E) Histological analysis of tumor isolated from different groups. Scale bars represent 25 μm.

major organs including heart, liver, spleen, and kidney (Figure S5).

4. CONCLUSIONS

We have shown that trastuzumab-decorated multifunctional polymersomal epirubicin (Tra-Ps-EPI) can be conveniently prepared with controllable Tra surface density, small size, high EPI loading, superb stability, HER2-targeting ability, and GSH-triggered intracellular drug release via post-ligand modification. Of note, Tra-Ps exhibits much stronger binding affinity to the HER2 extracellular domain than the native trastuzumab, with a 6-fold lower equilibrium dissociation constant. In accordance, Tra-Ps-EPI induces better cellular uptake and higher cytotoxicity in HER2-positive SKOV-3 cells than the non-targeted Ps-EPI to SKOV-3 cells and Tra-Ps-EPI to HER2-negative MDA-MB-231 cells. Moreover, Tra-Ps-EPI with high in vivo stability displays a long circulation time and deep tumor penetration, resulting in nearly complete tumor growth suppression and negligible systemic toxicity. These HER2-specific reduction-sensitive immunopolymersomes may provide an appealing strategy for targeted tumor chemotherapy.

■ ASSOCIATED CONTENT

Supporting Information

The Supporting Information is available free of charge on the ACS Publications website at DOI: 10.1021/acs.biomac.9b00947.

Details on materials, characterization, and cell culture; figures showing ^{1}H NMR spectra and GPC traces of PEG-P(TMC-DTC) and Mal-PEG-P(TMC-DTC) and SLS measurement of Mal-Ps; and characteristics of blank Ps with various Tra surface densities (PDF)

■ AUTHOR INFORMATION

Corresponding Authors

*E-mail: sunhuanli@suda.edu.cn (H.S.).
*E-mail: zyzhong@suda.edu.cn. Tel/Fax: +86-512-65880098 (Z.Z.).

ORCID

Huanli Sun: 0000-0001-6287-1555
Jeroen J. L. M. Cornelissen: 0000-0002-9728-5043
Zhiyuan Zhong: 0000-0003-4175-4741

Author Contributions

§L.D. and W.G. contributed equally to this work. The manuscript was written through contributions of all authors. All authors have given approval to the final version of the manuscript.

Notes

The authors declare no competing financial interest.

■ ACKNOWLEDGMENTS

This work was supported by the National Natural Science Foundation of China (51633005 and 51603138) and the Natural Science Foundation of Jiangsu Province (BK20160322).

■ REFERENCES

(1) Sliwkowski, M. X.; Mellman, I. Antibody therapeutics in cancer. *Science* **2013**, *341*, 1192−1198.
(2) Elgundi, Z.; Reslan, M.; Cruz, E.; Sifniotis, V.; Kayser, V. The state-of-play and future of antibody therapeutics. *Adv. Drug Delivery Rev.* **2017**, *122*, 2−19.
(3) Ayyar, B. V.; Arora, S.; O'Kennedy, R. Coming-of-age of antibodies in cancer therapeutics. *Trends Pharmacol. Sci.* **2016**, *37*, 1009−1028.
(4) Diamantis, N.; Banerji, U. Antibody-drug conjugates—an emerging class of cancer treatment. *Br. J. Cancer* **2016**, *114*, 362.
(5) Kulhari, H.; Pooja, D.; Rompicharla, S. V. K.; Sistla, R.; Adams, D. J. Biomedical applications of trastuzumab: As a therapeutic agent and a targeting ligand. *Med. Res. Rev.* **2015**, *35*, 849−876.
(6) Gemmete, J. J.; Mukherji, S. K. Trastuzumab (herceptin). *Am. J. Neuroradiol.* **2011**, *32*, 1373−1374.
(7) Parakh, S.; Gan, H. K.; Parslow, A. C.; Burvenich, I. J. G.; Burgess, A. W.; Scott, A. M. Evolution of anti-HER2 therapies for cancer treatment. *Cancer Treat. Rev.* **2017**, *59*, 1−21.
(8) Tai, W.; Mahato, R.; Cheng, K. The role of HER2 in cancer therapy and targeted drug delivery. *J. Controlled Release* **2010**, *146*, 264−275.
(9) Bryant, P.; Pabst, M.; Badescu, G.; Bird, M.; McDowell, W.; Jamieson, E.; Swierkosz, J.; Jurlewicz, K.; Tommasi, R.; Henseleit, K.; Sheng, X.; Camper, N.; Manin, A.; Kozakowska, K.; Peciak, K.; Laurine, E.; Grygorash, R.; Kyle, A.; Morris, D.; Parekh, V.; Abhilash, A.; Choi, J.-w.; Edwards, J.; Frigerio, M.; Baker, M. P.; Godwin, A. In vitro and in vivo evaluation of cysteine rebridged trastuzumab−MMAE antibody drug conjugates with defined drug-to-antibody ratios. *Mol. Pharmaceutics* **2015**, *12*, 1872−1879.
(10) Yao, Y.; Yu, L.; Su, X.; Wang, Y.; Li, W.; Wu, Y.; Cheng, X.; Zhang, H.; Wei, X.; Chen, H.; Zhang, R.; Gou, L.; Chen, X.; Xie, Y.; Zhang, B.; Zhang, Y.; Yang, J.; Wei, Y. Synthesis, characterization and targeting chemotherapy for ovarian cancer of trastuzumab-SN-38 conjugates. *J. Controlled Release* **2015**, *220*, 5−17.
(11) Amiri-Kordestani, L.; Blumenthal, G. M.; Xu, Q. C.; Zhang, L. J.; Tang, S. W. H.; Ha, L. N.; Weinberg, W. C.; Chi, B.; Candau-Chacon, R.; Hughes, P.; Russell, A. M.; Miksinski, S. P.; Chen, X. H.; McGuinn, W. D.; Palmby, T.; Schrieber, S. J.; Liu, Q.; Wang, J.; Song,

DOI: 10.1021/acs.biomac.9b00947
Biomacromolecules 2019, 20, 3855−3863

P. F.; Mehrotra, N.; Skarupa, L.; Clouse, K.; Al-Hakim, A.; Sridhara, R.; Ibrahim, A.; Justice, R.; Pazdur, R.; Cortazar, P. FDA approval: Ado-trastuzumab emtansine for the treatment of patients with HER2-positive metastatic breast cancer. *Clin. Cancer Res.* **2014**, *20*, 4436−4441.
(12) Beck, A.; Goetsch, L.; Dumontet, C.; Corvaïa, N. Strategies and challenges for the next generation of antibody−drug conjugates. *Nat. Rev. Drug Discov.* **2017**, *16*, 315−337.
(13) Lambert, J. M.; Berkenblit, A. Antibody−drug conjugates for cancer treatment. *Annu. Rev. Med.* **2018**, *69*, 191−207.
(14) Han, H.; Davis, M. E. Targeted nanoparticles assembled via complexation of boronic-acid-containing targeting moieties to diol-containing polymers. *Bioconjugate Chem.* **2013**, *24*, 669−677.
(15) Bahadur, K. C. R.; Chandrashekaran, V.; Cheng, B.; Chen, H.; Peña, M. M. O.; Zhang, J.; Montgomery, J.; Xu, P. Redox potential ultrasensitive nanoparticle for the targeted delivery of camptothecin to HER2-positive cancer cells. *Mol. Pharmaceutics* **2014**, *11*, 1897−1905.
(16) Vivek, R.; Thangam, R.; NipunBabu, V.; Rejeeth, C.; Sivasubramanian, S.; Gunasekaran, P.; Muthuchelian, K.; Kannan, S. Multifunctional HER2-antibody conjugated polymeric nanocarrier-based drug delivery system for multi-drug-resistant breast cancer therapy. *ACS Appl. Mater. Interfaces* **2014**, *6*, 6469−6480.
(17) Rong, L.; Zhou, S.; Liu, X.; Li, A.; Jing, T.; Liu, X.; Zhang, Y.; Cai, S.; Tang, X. Trastuzumab-modified DM1-loaded nanoparticles for $HER2^+$ breast cancer treatment: an *in vitro* and *in vivo* study. *Artif. Cells Nanomed. Biotechnol.* **2017**, *46*, 1708−1718.
(18) Sapra, P.; Shor, B. Monoclonal antibody-based therapies in cancer: Advances and challenges. *Pharmacol. Ther.* **2013**, *138*, 452−469.
(19) Sivaram, A. J.; Wardiana, A.; Howard, C. B.; Mahler, S. M.; Thurecht, K. J. Recent advances in the generation of antibody-nanomaterial conjugates. *Adv. Healthcare Mater.* **2018**, *7*, 1700607.
(20) Shargh, V. H.; Hondermarck, H.; Liang, M. Antibody-targeted biodegradable nanoparticles for cancer therapy. *Nanomedicine* **2016**, *11*, 63−79.
(21) Eloy, J. O.; Petrilli, R.; Chesca, D. L.; Saggioro, F. P.; Lee, R. J.; Marchetti, J. M. Anti-HER2 immunoliposomes for co-delivery of paclitaxel and rapamycin for breast cancer therapy. *Eur. J. Pharm. Biopharm.* **2017**, *115*, 159−167.
(22) Liu, Y.; Li, K.; Liu, B.; Feng, S.-S. A strategy for precision engineering of nanoparticles of biodegradable copolymers for quantitative control of targeted drug delivery. *Biomaterials* **2010**, *31*, 9145−9155.
(23) Zhao, J.; Feng, S.-S. Effects of PEG tethering chain length of vitamin E TPGS with a herceptin-functionalized nanoparticle formulation for targeted delivery of anticancer drugs. *Biomaterials* **2014**, *35*, 3340−3347.
(24) Choi, W. I.; Lee, J. H.; Kim, J.-Y.; Heo, S. U.; Jeong, Y. Y.; Kim, Y. H.; Tae, G. Targeted antitumor efficacy and imaging via multifunctional nano-carrier conjugated with anti-HER2 trastuzumab. *Nanomedicine* **2015**, *11*, 359−368.
(25) Sun, H.; Zhang, Y.; Zhong, Z. Reduction-sensitive polymeric nanomedicines: An emerging multifunctional platform for targeted cancer therapy. *Adv. Drug Delivery Rev.* **2018**, *132*, 16−32.
(26) Talelli, M.; Barz, M.; Rijcken, C. J. F.; Kiessling, F.; Hennink, W. E.; Lammers, T. Core-crosslinked polymeric micelles: Principles, preparation, biomedical applications and clinical translation. *Nano Today* **2015**, *10*, 93−117.
(27) Zhang, Y.; Ding, J.; Li, M.; Chen, X.; Xiao, C.; Zhuang, X.; Huang, Y.; Chen, X. One-step "click chemistry"-synthesized cross-linked prodrug nanogel for highly selective intracellular drug delivery and upregulated antitumor efficacy. *ACS Appl. Mater. Interfaces* **2016**, *8*, 10673−10682.
(28) Zou, Y.; Meng, F.; Deng, C.; Zhong, Z. Robust, tumor-homing and redox-sensitive polymersomal doxorubicin: A superior alternative to Doxil and Caelyx? *J. Controlled Release* **2016**, *239*, 149−158.
(29) Jiang, Y.; Yang, W.; Zhang, J.; Meng, F.; Zhong, Z. Protein toxin chaperoned by LRP-1-targeted virus-mimicking vesicles induces high-efficiency glioblastoma therapy in vivo. *Adv. Mater.* **2018**, *30*, 1800316.
(30) Zou, Y.; Zheng, M.; Yang, W.; Meng, F.; Miyata, K.; Kim, H. J.; Kataoka, K.; Zhong, Z. Virus-mimicking chimaeric polymersomes boost targeted cancer siRNA therapy in vivo. *Adv. Mater.* **2017**, *29*, 1703285.
(31) Yao, P.; Zhang, Y.; Meng, H.; Sun, H.; Zhong, Z. Smart polymersomes dually functionalized with cRGD and fusogenic GALA peptides enable specific and high-efficiency cytosolic delivery of apoptotic proteins. *Biomacromolecules* **2019**, *20*, 184−191.
(32) Xu, X.; Yang, W.; Liang, Q.; Shi, Y.; Zhang, W.; Wang, X.; Meng, F.; Zhong, Z.; Yin, L. Efficient and targeted drug/siRNA co-delivery mediated by reversibly crosslinked polymersomes toward anti-inflammatory treatment of ulcerative colitis (uc). *Nano Res.* **2019**, *12*, 659−667.
(33) Dai, Q.; Yan, Y.; Ang, C.-S.; Kempe, K.; Kamphuis, M. M. J.; Dodds, S. J.; Caruso, F. Monoclonal antibody-functionalized multilayered particles: Targeting cancer cells in the presence of protein coronas. *ACS Nano* **2015**, *9*, 2876−2885.
(34) Lale, S. V.; Kumar, A.; Prasad, S.; Bharti, A. C.; Koul, V. Folic acid and trastuzumab functionalized redox responsive polymersomes for intracellular doxorubicin delivery in breast cancer. *Biomacromolecules* **2015**, *16*, 1736−1752.
(35) Karra, N.; Nassar, T.; Ripin, A. N.; Schwob, O.; Borlak, J.; Benita, S. Antibody conjugated PLGA nanoparticles for targeted delivery of paclitaxel palmitate: Efficacy and biofate in a lung cancer mouse model. *Small* **2013**, *9*, 4221−4236.
(36) Schneider, C. S.; Perez, J. G.; Cheng, E.; Zhang, C.; Mastorakos, P.; Hanes, J.; Winkles, J. A.; Woodworth, G. F.; Kim, A. J. Minimizing the non-specific binding of nanoparticles to the brain enables active targeting of Fn14-positive glioblastoma cells. *Biomaterials* **2015**, *42*, 42−51.
(37) Zucker, D.; Marcus, D.; Barenholz, Y.; Goldblum, A. Liposome drugs' loading efficiency: A working model based on loading conditions and drug's physicochemical properties. *J. Controlled Release* **2009**, *139*, 73−80.
(38) Li, X.; Hirsh, D. J.; Cabral-Lilly, D.; Zirkel, A.; Gruner, S. M.; Janoff, A. S.; Perkins, W. R. Doxorubicin physical state in solution and inside liposomes loaded via a pH gradient. *Biochim. Biophys. Acta, Biomembr.* **1998**, *1415*, 23−40.
(39) Nakamura, H.; Koziolová, E.; Chytil, P.; Tsukigawa, K.; Fang, J.; Haratake, M.; Ulbrich, K.; Etrych, T.; Maeda, H. Pronounced cellular uptake of pirarubicin versus that of other anthracyclines: Comparison of HPMA copolymer conjugates of pirarubicin and doxorubicin. *Mol. Pharmaceutics* **2016**, *13*, 4106−4115.
(40) Launchbury, A. P.; Habboubi, N. Epirubicin and doxorubicin - a comparison of their characteristics, therapeutic activity and toxicity. *Cancer Treat. Rev.* **1993**, *19*, 197−228.
(41) Xue, S.; Gu, X.; Zhang, J.; Sun, H.; Deng, C.; Zhong, Z. Construction of small-sized, robust, and reduction-responsive polypeptide micelles for high loading and targeted delivery of chemotherapeutics. *Biomacromolecules* **2018**, *19*, 3586−3593.
(42) Liu, M.; Khan, A. R.; Ji, J.; Lin, G.; Zhao, X.; Zhai, G. Crosslinked self-assembled nanoparticles for chemo-sonodynamic combination therapy favoring antitumor, antimetastasis management and immune responses. *J. Controlled Release* **2018**, *290*, 150−164.
(43) Hsueh, S.-P.; Du, J.-L.; Hsu, W.-B.; Fang, C.-A.; Liu, H.; Wang, W.-B. SV40 T/t-common polypeptide enhances the sensitivity of HER2-overexpressing human cancer cells to anticancer drugs cisplatin and doxorubicin. *Cancer Lett.* **2012**, *324*, 48−57.
(44) Ding, L.; Tian, C.; Feng, S.; Fida, G.; Zhang, C.; Ma, Y.; Ai, G.; Achilefu, S.; Gu, Y. Small sized EGFR1 and HER2 specific bifunctional antibody for targeted cancer therapy. *Theranostics* **2015**, *5*, 378−398.
(45) Pruszynski, M.; D'Huyvetter, M.; Bruchertseifer, F.; Morgenstern, A.; Lahoutte, T. Evaluation of an anti-HER2 nanobody labeled with 225Ac for targeted α-particle therapy of cancer. *Mol. Pharmaceutics* **2018**, *15*, 1457−1466.

DOI: 10.1021/acs.biomac.9b00947
Biomacromolecules 2019, 20, 3855−3863

(46) Magnifico, A.; Albano, L.; Campaner, S.; Delia, D.; Castiglioni, F.; Gasparini, P.; Sozzi, G.; Fontanella, E.; Menard, S.; Tagliabue, E. Tumor-initiating cells of HER2-positive carcinoma cell lines express the highest oncoprotein levels and are sensitive to trastuzumab. *Clin. Cancer Res.* **2009**, *15*, 2010−2021.
(47) Li, W.-M.; Chiang, C.-S.; Huang, W.-C.; Su, C.-W.; Chiang, M.-Y.; Chen, J.-Y.; Chen, S.-Y. Amifostine-conjugated pH-sensitive calcium phosphate-covered magnetic-amphiphilic gelatin nanoparticles for controlled intracellular dual drug release for dual-targeting in HER-2-overexpressing breast cancer. *J. Controlled Release* **2015**, *220*, 107−118.
(48) Liu, T.; Lai, L.; Song, Z.; Chen, T. A sequentially triggered nanosystem for precise drug delivery and simultaneous inhibition of cancer growth, migration, and invasion. *Adv. Funct. Mater.* **2016**, *26*, 7775−7790.
(49) Vivek, R.; Thangam, R.; Kumar, S. R.; Rejeeth, C.; Sivasubramanian, S.; Vincent, S.; Gopi, D.; Kannan, S. HER2 targeted breast cancer therapy with switchable "off/on" multifunctional "smart" magnetic polymer core−shell nanocomposites. *ACS Appl. Mater. Interfaces* **2016**, *8*, 2262−2279.
(50) Guo, Y.; Wang, X.-Y.; Chen, Y.-L.; Liu, F.-Q.; Tan, M.-X.; Ao, M.; Yu, J.-H.; Ran, H.-T.; Wang, Z.-X. A light-controllable specific drug delivery nanoplatform for targeted bimodal imaging-guided photothermal/chemo synergistic cancer therapy. *Acta Biomater.* **2018**, *80*, 308−326.
(51) Ngamcherdtrakul, W.; Morry, J.; Gu, S.; Castro, D. J.; Goodyear, S. M.; Sangvanich, T.; Reda, M. M.; Lee, R.; Mihelic, S. A.; Beckman, B. L.; Hu, Z.; Gray, J. W.; Yantasee, W. Cationic polymer modified mesoporous silica nanoparticles for targeted siRNA delivery to HER2+ breast cancer. *Adv. Funct. Mater.* **2015**, *25*, 2646−2659.
(52) Wilken, J. A.; Webster, K. T.; Maihle, N. J. Trastuzumab sensitizes ovarian cancer cells to EGFR-targeted therapeutics. *J. Ovarian Res.* **2010**, *3*, 7.
(53) Chen, J.; Huang, K.; Chen, Q.; Deng, C.; Zhang, J.; Zhong, Z. Tailor-making fluorescent hyaluronic acid microgels via combining microfluidics and photoclick chemistry for sustained and localized delivery of herceptin in tumors. *ACS Appl. Mater. Interfaces* **2018**, *10*, 3929−3937.
(54) Fang, Y.; Yang, W.; Cheng, L.; Meng, F.; Zhang, J.; Zhong, Z. EGFR-targeted multifunctional polymersomal doxorubicin induces selective and potent suppression of orthotopic human liver cancer in vivo. *Acta Biomater.* **2017**, *64*, 323−333.
(55) Yang, W.; Wei, Y.; Yang, L.; Zhang, J.; Zhong, Z.; Storm, G.; Meng, F. Granzyme B-loaded, cell-selective penetrating and reduction-responsive polymersomes effectively inhibit progression of orthotopic human lung tumor in vivo. *J. Controlled Release* **2018**, *290*, 141−149.
(56) Gandhi, R.; Khatri, N.; Baradia, D.; Vhora, I.; Misra, A. Surface-modified epirubicin-HCl liposomes and its in vitro assessment in breast cancer cell-line: MCF-7. *Drug Delivery* **2016**, *23*, 1152−1162.
(57) Zhang, T.; Zhou, S.; Hu, L.; Peng, B.; Liu, Y.; Luo, X.; Song, Y.; Liu, X.; Deng, Y. Polysialic acid-modifying liposomes for efficient delivery of epirubicin, in-vitro characterization and in-vivo evaluation. *Int. J. Pharm.* **2016**, *515*, 449−459.
(58) Shi, J.; Kantoff, P. W.; Wooster, R.; Farokhzad, O. C. Cancer nanomedicine: Progress, challenges and opportunities. *Nat. Rev. Cancer* **2017**, *17*, 20−37.
(59) Sun, Q.; Zhou, Z.; Qiu, N.; Shen, Y. Rational design of cancer nanomedicine: Nanoproperty integration and synchronization. *Adv. Mater.* **2017**, *29*, 1606628.
(60) Anchordoquy, T. J.; Barenholz, Y.; Boraschi, D.; Chorny, M.; Decuzzi, P.; Dobrovolskaia, M. A.; Farhangrazi, Z. S.; Farrell, D.; Gabizon, A.; Ghandehari, H.; Godin, B.; La-Beck, N. M.; Ljubimova, J.; Moghimi, S. M.; Pagliaro, L.; Park, J.-H.; Peer, D.; Ruoslahti, E.; Serkova, N. J.; Simberg, D. Mechanisms and barriers in cancer nanomedicine: Addressing challenges, looking for solutions. *ACS Nano* **2017**, *11*, 12−18.
(61) Sun, Q.; Ojha, T.; Kiessling, F.; Lammers, T.; Shi, Y. Enhancing tumor penetration of nanomedicines. *Biomacromolecules* **2017**, *18*, 1449−1459.
(62) Wang, S.; Shin, I. S.; Hancock, H.; Jang, B.-S.; Kim, H.-S.; Lee, S. M.; Zderic, V.; Frenkel, V.; Pastan, I.; Paik, C. H.; Dreher, M. R. Pulsed high intensity focused ultrasound increases penetration and therapeutic efficacy of monoclonal antibodies in murine xenograft tumors. *J. Controlled Release* **2012**, *162*, 218−224.
(63) Wang, Y.; Liu, P.; Qiu, L.; Sun, Y.; Zhu, M.; Gu, L.; Di, W.; Duan, Y. Toxicity and therapy of cisplatin-loaded EGF modified mPEG-PLGA-PLL nanoparticles for SKOV3 cancer in mice. *Biomaterials* **2013**, *34*, 4068−4077.
(64) Zou, Y.; Xia, Y.; Meng, F.; Zhang, J.; Zhong, Z. GE11-directed functional polymersomal doxorubicin as an advanced alternative to clinical liposomal formulation for ovarian cancer treatment. *Mol. Pharmaceutics* **2018**, *15*, 3664−3671.
(65) Bae, K. H.; Tan, S.; Yamashita, A.; Ang, W. X.; Gao, S. J.; Wang, S.; Chung, J. E.; Kurisawa, M. Hyaluronic acid-green tea catechin micellar nanocomplexes: Fail-safe cisplatin nanomedicine for the treatment of ovarian cancer without off-target toxicity. *Biomaterials* **2017**, *148*, 41−53.
(66) Wang, Y.; Liu, P.; Duan, Y.; Yin, X.; Wang, Q.; Liu, X.; Wang, X.; Zhou, J.; Wang, W.; Qiu, L.; Di, W. Specific cell targeting with APRPG conjugated PEG−PLGA nanoparticles for treating ovarian cancer. *Biomaterials* **2014**, *35*, 983−992.

DOI: 10.1021/acs.biomac.9b00947
Biomacromolecules 2019, 20, 3855−3863